Pilot neuromusculoskeletal system bond graph

Résumé long du chapitre 3

Dans le chapitre précédent, un modèle aéromécanique d'hélicoptère a été développé. Dans ce chapitre, un modèle neuro-musculo-squelettique du bras droit du pilote est développé. Le caractère prédictif du modèle est discuté en le comparant à des résultats expérimentaux disponibles dans la littérature.
Une revue des modèles de pilotes d'aéronef à voilure fixe est proposée dans (McRuer & Jex, 1967) *; celle-ci conduit McRuer à développer pendant des années son travail sur les interactions homme-machine dont un aperçu est donné dans* (McRuer, 1980)*. Concentré sur les oscillations induites par les pilotes d'aéronefs,* (McRuer, 1995) *distingue trois comportements principaux chez les pilotes qui sont : le suivi de trajectoire, la compensation et l'anticipation. Le comportement compensatoire, peut-être visualisé, en imaginant, par exemple, l'attitude d'un pilote d'hélicoptère pendant un ravitaillement air-air en carburant. Le comportement d'anticipation correspond lui aux actions prises par le pilote par anticipation du comportement dynamique de la machine qu'il contrôle et en se basant sur son expérience. Dans* (Lone & Cooke, 2010) *et* (Lone & Cooke, 2014)*, une vision du pilote plutôt du point de vue de l'ingénieur est proposée. En effet, les auteurs décomposent les modèles de pilote en trois catégories : sensorielle (capteurs), de contrôle (lois de commande) et biomécanique (actionneurs), voir la Figure 3-1. Des combinaisons de ces différents modèles permettent d'étudier les oscillations induites par le pilote (PIO) et assistées par le pilote (PAO). Si l'on se restreint aux PAOs,* (McRuer, 1995) *dresse une liste d'incidents survenus sur des avions comme le YF-12 de Lockheed ou le F-111 de General Dynamics. Sur les avions de chasse, le phénomène le plus étudié dans la littérature ouverte est probablement le PAO connu sous le nom de « roll rachet »*. (Hess, 1998) *et* (Höhne, 2000) *décrivent le phénomène comme « des oscillations indésirables et imprévues à haute fréquence sur l'axe de roulis d'avions de chasse de haute performance qui apparaissent lors de manœuvres rapides en roulis »*. (Höhne, 2000) *déclare qu'il est désormais accepté, que le phénomène de « roll rachet » est influencé par le système neuromusculaire des pilotes. Dans ses travaux, il propose un modèle biomécanique du pilote couplé à un modèle d'aéronef afin d'étudier le phénomène et grâce auquel il arrive à reproduire numériquement un incident survenu sur un F16 du constructeur General Dynamics. Ce phénomène est aussi reporté pour être survenu sur un Eurofighter Typhoon,* (Lone & Cooke, 2014)*. Dans la communauté des aéronefs à voilure tournante, une revue d'incidents survenue dans la US Navy et le corps des Marines est rapporté dans* (Walden, 2007)*. On y trouve un grand nombre d'appareils touchés par le phénomène de PAO ou RPC aéroélastique.* (Walden, 2007) *cite un exemple aux conséquences impressionnantes à propos de l'hélicoptère CH-53 Super Stallion du constructeur Sikorsky, voir Figure 3-2.*

Walden rapporte qu'un véhicule militaire qui était transporté à l'aide d'une élingue par l'hélicoptère a dû être largué pendant le vol à cause de l'émergence très violente du phénomène de 'vertical collective bounce'. Afin de mieux comprendre le problème, (Mayo, 1989) *propose le premier modèle à être utilisé dans l'industrie et représentant la biodynamique d'un pilote d'hélicoptère. Ce modèle linéaire, voir Figure 3-3, a été obtenu par identification à partir d'expériences menées dans le simulateur de vol du constructeur Sikorsky. L'expérience consistait à enregistrer le mouvement du manche de pas collectif imposé par un pilote alors que la plateforme du simulateur oscillait verticalement de manière forcée à des fréquences entre 1 et 5 Hz. Ceci a permis d'obtenir la transmissibilité du pilote selon leurs morphologies : mésomorphe ou ectomorphe. Comme nous l'avons déjà précisé en introduction, ce comportement de la part du pilote est un comportement au-dessus des fréquences de contrôle manuel d'un véhicule. Par conséquent, il est considéré comme un comportement involontaire du pilote. De plus, il est facile d'imaginer que ce type de comportement peut apparaître sur d'autres types de véhicules que des aéronefs. La fonction qui caractérise ce comportement a été formalisée par* (Venrooij, 2014) *sous le nom de* ***« biodynamic feedthrough » (BDFT)*** *et il l'a défini comme « **le transfert d'accélérations par le corps humain pendant l'exécution d'une tâche de contrôle manuel, qui engendre des forces involontaires qui s'appliquent sur le dispositif de commande, et qui peut éventuellement provoquer des mouvements involontaires du dispositif de commande** ». Les expériences de* (Mayo, 1989) *montrent Figure 3-3 que le BDFT est variable en fonction des pilotes, de par leur morphologie. Mais le BDFT est également variable chez un même pilote ; en effet les pilotes adaptent leurs actions et donc leur 'corps' en fonction des tâches qui leurs sont demandées d'effectuer, de leur charge de travail et de leur état de fatigue* (Venrooij, 2014). *En effet, lors d'expériences menées sur le simulateur de vol Simona de l'université technologique de Delft (TU Delft), par Venrooij, il a été demandé à chaque pilote d'effectuer trois types de tâches différentes alors que la plateforme du simulateur vibrait dans le but de mesurer leur BDFT. L'objectif derrière la demande d'effectuer des tâches différentes étaient de forcer chaque pilote à réadapter son système neuromusculaire à chaque tâche. Les résultats sont présentés sur la Figure 3-4 sur les axes latéral, longitudinal et vertical de l'hélicoptère. Il apparaît assez clairement que le BDFT dépend de la tâche effectuée par chaque pilote. Une des conclusions principales de* (Venrooij, 2014) *est que la fréquence de résonance du BDFT est la plus haute lorsque la tâche demandée au pilote le force à devenir plus 'raide' lorsqu'il agit sur les commandes. Des conclusions similaires sont rapportées dans* (Lone & Cooke, 2014) *qui précisent que ce type de comportements peut être atteint lors de situations d'urgence notamment. Dès lors, il apparaît nécessaire de pouvoir représenter l'adaptation du système neuromusculaire d'un pilote. Deux types d'approches ont été identifiés dans la littérature afin de modéliser le comportement biodynamique des pilotes. La première consiste à identifier la réponse du corps humain à des accélérations dans le domaine fréquentiel à partir d'expériences* (Mayo, 1989), (Venrooij, et al., 2011) *et* (Muscarello, et al., 2015). *La deuxième approche consiste à tenter de prédire le BDFT en déduisant les mouvements en se basant sur des principes physiques, par exemple en utilisant une approche multicorps afin de modéliser le squelette humain sur lequel on superpose des modèles dynamiques de*

muscles ainsi que, dans une certaine mesure, du système nerveux central (Masarati & Quaranta, 2014)*. C'est la voie ouverte par ces travaux, basée sur des principes physiques, que nous prenons afin d'obtenir un modèle prédictif dans un grand nombre de mises en situations virtuelles. L'état de l'art des modèles dits « neuro-musculo-squelettique » est très vaste dans le domaine de la biomécanique, on peut citer notamment* (Maurel, 1999), (Pandy, 2001), (Garner & Pandy, 2001), (Lee & Terzopoulos, 2006), (Pennestri, Stefanelli, Valentini, & Vita, 2007), (Erdemir, McLean, Herzog, & van den Bogert, 2007), (Hernani, Romero, & Jazmati, 2011) *ou encore* (Masarati & Quaranta, 2014). *Ce type de modèles, basés sur des principes physiques, peut être appliqué à l'étude d'un nombre de situations virtuelles bien plus vastes et dans un nombre de domaine bien plus important que les modèles obtenus par identification, valables eux, uniquement dans les conditions expérimentales à partir desquelles ils ont été obtenus.*

Il n'y a pas, à l'heure actuelle, de consensus sur comment prédire le BDFT par le calcul à partir d'un modèle neuro-musculo-squelettique. Il est proposé ici de développer un tel modèle, du bras droit du pilote à partir de modèles existants dans la littérature et notamment à partir des travaux répertoriés dans le paragraphe précédent. Le modèle proposé est néanmoins original pour deux raisons. La première est qu'il est développé à l'aide de bond graphs ; il existe des modèles multicorps squelettiques en bond graphs, mais pas de modèle neuro –musculo-squelettique. La deuxième raison est qu'il est capable de tenir compte de mouvements spatiaux du squelette. Ceci est nécessaire dans notre application, puisque nous souhaitons être capable de calculer les mouvements sur l'axe latéral d'un cockpit d'hélicoptère. Le modèle proposé ici contient 16 muscles et le bras est décomposé en 2 os : un ensemble radius et cubitus d'une part et l'humérus d'autre part, voir Figure 3-7 et la Table 4, ainsi que Appendix 4 pour les données et définitions des repères.

Si l'on considère le système bras et manche de pas cyclique, ceux-ci sont attachés à un même solide : le fuselage. Par conséquent, le système est cinématiquement bouclé, voir Figure 3-8. Le modèle mathématique derrière un tel système peut-être difficile à résoudre numériquement. Une méthode connue sous le nom des « perturbations singulières » (Zeid & Overholt, 1995), (Boudon, 2014) *permet de transformer le modèle mathématique afin de faciliter sa résolution numérique. La méthode consiste à 'assouplir' au moins une contrainte de la boucle cinématique au niveau d'une liaison par l'ajout d'éléments de raideur (C) et de dissipation (R) linéaires. Il est choisi dans ce cas d'application, d'assouplir la contrainte au niveau de la liaison pivot entre le manche de pas cyclique et le fuselage, voir Figure 3-9. Cette méthode possède l'avantage d'être systématique et peut-être implémentée directement au niveau graphique d'un bond graph. Afin que le modèle reste physiquement valide, le choix des valeurs des éléments (C) et (R) peut se faire en identifiant la raideur et l'amortissement de la liaison du système physique. La méthode a le désavantage d'introduire de nouvelles variables d'état et donc de venir potentiellement perturber l'analyse du système par la prise en compte de modes indésirables.*

Le modèle squelettique est un modèle multicorps sur lequel il est nécessaire de superposer les muscles. Parmi les modèles comportementaux des muscles, on trouve le plus classique qui est le modèle de Hill, voir (Zajac, 1988)*, tenant compte de l'activation musculaire voir* (Pennestri, Stefanelli, Valentini, & Vita, 2007). *Ce*

dernier est traduit ici en bond graphs, équations (37) à (54) et permet d'aboutir à la structure graphique d'un muscle voir, Figure 3-12. Sur cette même figure, on voit apparaître en gris, des signaux qui vont vers et viennent du système nerveux central (CNS). Physiologiquement parlant, des 'capteurs' placés sur les fibres musculaires envoient une information sur l'état d'élongation des fibres en question ; c'est ainsi que le corps humain peut réguler la contraction ou la décontraction des muscles pour réaliser un mouvement ou maintenir une posture donnée. En effet, une posture peut être maintenue avec différents niveaux d'activations musculaires. Afin de mieux comprendre ceci, on peut s'imaginer avec un verre à la main ; il est possible de tenir ce verre plus ou moins fermement. Cette fermeté donne une idée du niveau d'activation musculaire : plus le verre est tenu fermement, plus l'activation est élevée. Ceci est formalisé mathématiquement par la quantité a, qui module la force produite par un muscle, voir équation (39) et Figure 3-10. De plus, on peut voir que la force musculaire, comme prévue par le modèle de Hill dépend de l'élongation du muscle (fonctions f_1 et f_3) et de sa vitesse d'élongation (fonction f_2). Un modèle quasi-statique du système nerveux central est également reproduit, (Lee & Terzopoulos, 2006), *afin de représenter le contrôle par le CNS, des forces musculaires. Cette modélisation consiste à ajouter le terme Δa à l'activation musculaire initiale a_0, voir l'équation (56). Deux coefficients apparaissent, k_p et k_v qui permettent de paramétrer l'état plus ou moins 'raide' du système neuromusculaire.*

Le modèle neuro-musculo-squelettique ainsi obtenu possède plus de muscles (16) que de degrés de liberté (9). Le système est donc sur-actionné ; mathématiquement le système possède plus d'inconnues que d'équations. En l'état, le système d'équations ne possède aucune, ou une infinité de solutions, (Pandy, 2001), (Erdemir, McLean, Herzog, & van den Bogert, 2007). *Afin de lever le problème d'indétermination, un principe physique supplémentaire est en général pris en compte. Par exemple, on peut postuler, afin de réaliser un mouvement ou de maintenir une posture donnée, que le corps humain minimise l'énergie consommée, appelée coût métabolique, par ses muscles,* (Erdemir, McLean, Herzog, & van den Bogert, 2007). *A partir de la modélisation précédente nous avons accès au travail mécanique fournit par chaque muscle, voir équation (55). Cette quantité ne représente pas tout à fait le coût métabolique ; en effet, lorsqu'un muscle travaille il dissipe une quantité d'énergie non négligeable sous forme de chaleur. Néanmoins, il est assumé qu'il est acceptable de minimiser le travail des muscles lorsque l'on cherche à minimiser le coût métabolique. La minimisation du travail des forces des muscles est prise en compte afin d'obtenir les coefficients d'activation musculaire initiaux a_0 des muscles. Pour cela, le modèle neuro-musculo-squelettique est implémenté dans le logiciel 20-sim ® et couplé au logiciel Matlab ® afin de pouvoir utiliser un algorithme d'optimisation, voir* Figure 3-15. *Le modèle est simulé au voisinage de l'équilibre, manche de pas cyclique droit, c'est-à-dire lorsque le pilote maintien cette posture. En paramétrant comme conditions initiales un angle de manche de pas cyclique légèrement décalé de sa valeur à l'équilibre et des coefficients a_0 nuls, on obtient un résultat de simulation de la réponse libre du système ; en quelques secondes, les oscillations s'atténuent et le système atteint l'équilibre. Cette opération donne une première valeur à la fonction coût qui est par la suite envoyée à la fonction d'optimisation, sous Matlab*

®, *qui propose un nouvel ensemble de coefficients d'activations musculaires. Par itération, on obtient un jeu de coefficients optimaux.*

La dernière étape de ce chapitre consiste à discuter de la validité du modèle. Il est proposé de reproduire les expériences réalisées sur le simulateur Simona de l'université technologique de Delft et dont les résultats ont été présentés Figure 3-4*. Dans ces expériences, il est demandé à chaque pilote d'effectuer 3 tâches différentes dans le cockpit alors que celui-ci vibre. Les vibrations qui nous intéressent sont notamment celles sur l'axe latéral de l'hélicoptère. La première tâche qui est demandée d'effectuer à chaque pilote est une tâche dite de « position » : le pilote doit par des mouvements de manche placer un curseur dans une cible qui se déplace sur l'écran du simulateur. La deuxième tâche est dite de « force » : le pilote doit chercher d'abord à contrer les forces qu'il ressent au manche avant de chercher à positionner le curseur sur la cible. La dernière tâche dite « relax » consiste à maintenir le manche dans sa position initiale en gardant un état des muscles proches de l'état initial sans forcément cherche à positionner le curseur dans la cible. Les résultats* Figure 3-4 *montrent que le BDFT dépend de la tâche qu'un pilote doit effectuer et donc de l'état de son système neuromusculaire ; le pilote semble notamment plus 'raide' lors des tâches du type « position ». Afin de pouvoir reproduire différents types d'état du système neuromusculaire par la simulation du modèle proposé, nous avons introduit le modèle quasi-statique du système nerveux central qui est paramétré par deux coefficients k_p et k_v,* (Stroeve, 1999), (Masarati & Quaranta, 2014). *Il n'y a pas de consensus dans la littérature sur la valeur à donner à ses coefficients selon la tâche que l'on demande d'effectuer à un pilote. Dans les présents travaux nous ne faisons varier que k_p, qui correspond au gain de la boucle de contrôle du coefficient d'activation musculaire pour la partie qui dépend de l'élongation d'un muscle. Ici un seul coefficient paramètre tous les muscles. De plus, on se permet de modifier la raideur et l'amortissement de deux articulations du modèle de bras, au niveau de l'épaule et du poignet. Ceci est fait par l'intermédiaire d'un coefficient multiplicateur des valeurs nominales de raideur et d'amortissement noté α.*
En se fixant des valeurs de k_p et α qui imposent un état neuromusculaire donné, on peut par l'opération d'optimisation décrite précédemment calculer les coefficients d'activation musculaire optimisés pour l'état neuromusculaire donné. Les résultats sont présentés Figure 3-16*. A partir de ces résultats, deux des jeux de paramètres sont choisis et une simulation, de la réponse forcée du bras pilote sur le manche de pas cyclique est menée pour des excitations en accélération latérale du cockpit d'amplitude constante et de fréquence variable entre 0.8 et 8 Hz. Une approximation des moindres carrées des résultats est effectuée et les résultats sont tracés sur la* Figure 3-17*, puis superposés aux résultats expérimentaux de* (Venrooij, et al., 2011). *La correspondance des résultats est très encourageante, les tâches de « force » et de « position » ont été reproduites par le calcul numérique. Il reste néanmoins encore des points d'amélioration. Le premier concerne la modification du paramètre α, qui paramètre la raideur et l'amortissement du bras aux interfaces. Il serait intéressant de voir si ce coefficient peut être remplacé par la modélisation d'un nombre encore plus important de muscles aux interfaces, comme par exemple le muscle deltoïde de l'épaule, voir* Figure 3-21*. Un dernier*

point qui n'a pas été abordé est que lorsque le coefficient k_p=1.25, le modèle présente un comportement non linéaire très fort à basse fréquence, voir le spectrogramme Figure 3-20 *: des harmoniques apparaissent et leur amplitude est importante. Les résultats de simulation de BDFT présentés* Figure 3-17 *et par les résultats expérimentaux de la littérature ne représentent donc qu'une partie de la réponse biodynamique du pilote : celle aux fréquences d'excitations.*

In addition to the rotorcraft model presented in the previous section, the development of a pilot model is presented in this section. The objective of this model is to be able to predict pilot's involuntary behavior known as *biodynamic feedthrough* (BDFT) on the lateral axis of a helicopter cockpit. The model is in the last section confronted to literature flight simulator experiment results.

3.1. State-of-the art

An early review of pilot models is proposed in (McRuer & Jex, 1967); it lead McRuer to extensive work around human dynamics in man-machine systems in (McRuer, Human dynamics in man-machine systems, 1980). Mainly concentrated on aircraft pilot induced oscillations, (McRuer, 1995) distinguishes three main pilot behavioral descriptions which are trajectory following, compensation and precognitive. The compensation behavior could be imagined as the one an aircraft or helicopter pilot would have during an air to air refueling operation. It usually demands fast and short term actions from the pilot. The precognitive behavior concerns anticipative actions based on experience taken by the pilot to make the aircraft reach a desired state. In (Lone & Cooke, 2010), (Lone & Cooke, 2014) review pilot modeling techniques and propose to represent such behavior by discretizing the pilot models into three model categories: sensory models, control models, and biomechanical models see Figure 3-1. The human sensory models represent the dynamics between the inputs of visual cues (through the primary flight display, out of the window cues), the proprioception (cyclic lever see Figure 2, collective lever and pedals positions) and finally the vestibular system (sensing body motion - inner ear) and outputs that are communicated to higher brain functions for processing. Once the brain has processed the information, it sends a decision, also influenced by experience and skills, to the 'actuation system' of the human body, its neuromuscular system.

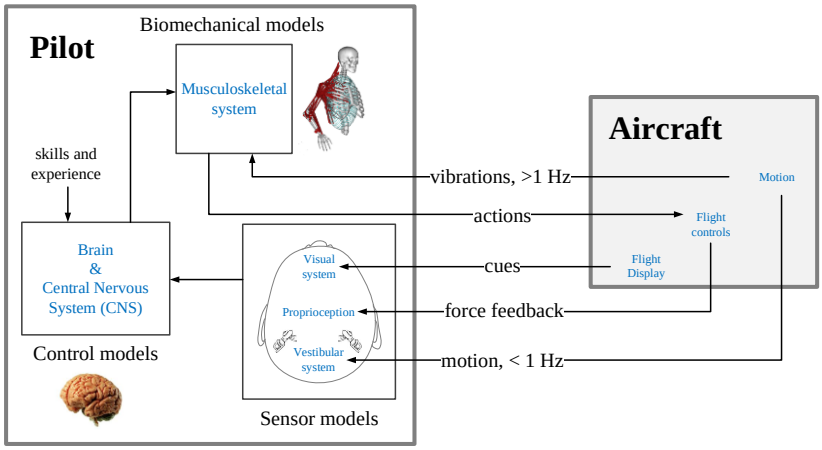

Figure 3-1. Pilot submodels in human-aircraft systems, adapted from (Lone & Cooke, 2014)

This thesis focuses on the pilot interaction with higher frequency helicopters modes also known as aeroelastic RPCs or pilot assisted oscillations (PAOs). A list of incidents is reported in (McRuer, 1995), in which aircrafts such as Lockheed YF-12 or General Dynamics F-111 have been involved in a PAO. Perhaps the most studied phenomena in the open literature concerning aircrafts is the 'roll ratchet' phenomena (Hess, 1998), which is "*an unwanted and inadvertent high frequency oscillation in the roll axis encountered in high performance fighter aircraft during rapid roll maneuvers*" (Höhne, 2000). The same author points out that "*it is widely accepted that roll ratchet is influenced by the pilot's neuromuscular system*" and proposes a biomechanical model of the pilot coupled to an aircraft model to investigate the phenomena. It successfully reproduced the incident on General Dynamics F16. This phenomena is also known to have appeared on Eurofighter Typhoon (Lone & Cooke, 2014).

In the rotorcraft community, an extensive list of incidents associated to rotorcraft PAOs in the US Navy and Marine Corps is presented by (Walden, 2007). Tiltrotor designs such as the Boeing-Bell V-22 Osprey were very sensitive to PAOs, for which three unstable aeroelastic RPCs in its lateral axis were found after flight testing in (Parham, Popelka, Miller, & Froebel, 1991). The first two modes appeared while on the ground while the last one appeared in the air at high speed. The mechanism behind the first two modes was found to be due to a difference of thrust between the two rotors that was the result of an output of the flight control system due to the involuntary movement of the lateral lever by the pilot. A PAO tendency of conventional helicopters that has been widely studied in the community is the 'vertical collective bounce phenomena' for which Sikorsky's CH-53 Super Stallion was prone when transporting a slung load see Figure 3-2. It is reported in (Walden, 2007) that the load at the end of the cable, a light armored vehicle had once during an incident to be jettisoned.

Figure 3-2. Sikorsky CH-53E Super Stallion with external slung load

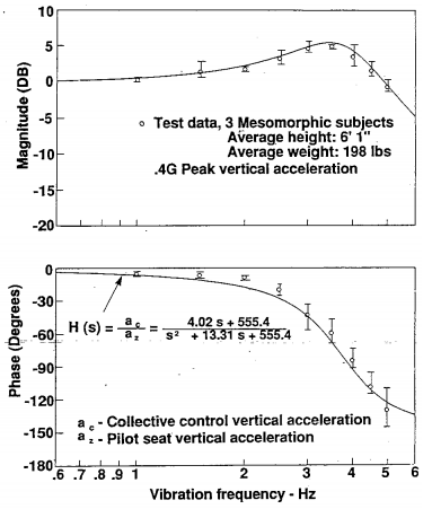

Figure 3-3. Pilot transmissibility experiment from (Mayo, 1989)

In order to better understand the problem and design a solution, (Mayo, 1989) proposed one of the first pilot biodynamics model to be used in industry. This model was obtained by identifications from experiments conducted on one of Sikorsky's motion-based simulators. The experiment consisted in recording pilot's collective stick motion while vertical sinusoidal commands were applied to the simulator platform at discrete frequencies ranging from 1 to 5 Hz (see Figure 3-3). It allowed to obtain the transmissibility of different pilots based on their body shapes: mesomorph or ectomorph. This behavior represents an involuntary behavior of the pilots that arises at higher frequencies than those of manual control, in the present example around 3Hz. This behavior is not restricted to aircrafts or rotorcrafts but can appear in any man-machine system and it is usually called *biodynamic feedthrough* (BDFT). A framework to measure BDFT and its definition proposed by (Venrooij, 2014): "*the transfer of accelerations through the human body during the execution of a manual control task, causing involuntary forces being applied to the control device, which may result in involuntary control device deflections*". BDFT therefore explains that when a pilot is engaged in a manual control task under vehicle accelerations, these vibrations can cause involuntary limb motions leading to involuntary control inputs. The experiments presented by (Mayo, 1989) on Figure 3-3 show that BDFT varies between different subjects. Furthermore it is known that pilots adapt their response and therefore their bodies to task instruction, workload and fatigue (Venrooij, 2014). In that same work, BDFT responses of humans were measured when asked to perform different control tasks. The objective of asking one subject to perform different tasks is to force him to adapt his body and therefore his neuromuscular system to the task. The results are presented on Figure 3-4 for the lateral, longitudinal and vertical helicopter axis translations and show that BDFT is also task dependent. These experimental results from (Venrooij, 2014) were obtained on TU Delft's experimental motion based simulator, for which the subjects were asked to perform three tasks. A position task (PT) with the instruction to minimize the stick position, a force task (FT)

with the instruction to minimize the force applied to the stick and finally a relax task (RT) with the instruction to relax the arm.

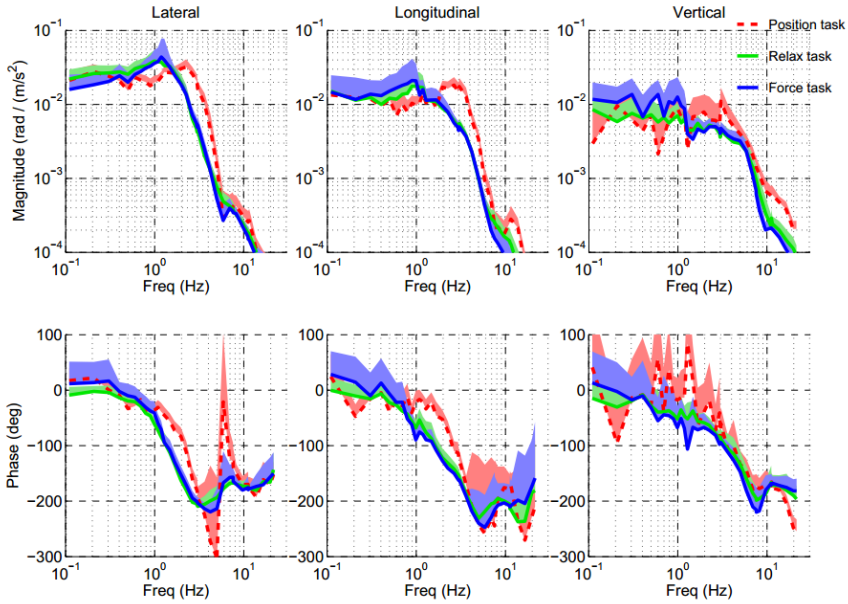

Figure 3-4. Biodynamic feedthrough task dependency, helicopter flight simulator experiments, from (Venrooij, 2014)

From the frequency responses of Figure 3-4, it appears that for position tasks (PT) the resonant peak of BDFT is higher. The conclusions drawn in (Venrooij, 2014) are that the position task is the one that requires the higher stiffness adaption of the neuromuscular system. Similar conclusions are reported in (Lone & Cooke, 2014) and especially that the body 'stiffens' during urgent tracking tasks.

As a result, the main relevant behavior to model BDFT is the neuromuscular system adaption of the pilot. When modeling pilot biodynamics, two approaches can be identified. The first one consists in identifying the human body response in the frequency domain to fuselage accelerations from experiments (Mayo, 1989), (Venrooij, et al., 2011) and (Muscarello, et al., 2015) to name a few. The second approach consists in trying to predict biodynamic feedthrough by deducing the motion based on physical principles using for example a multibody approach to capture the skeletal motion superposed to dynamic models of the muscles and central nervous system control (Masarati & Quaranta, 2014).

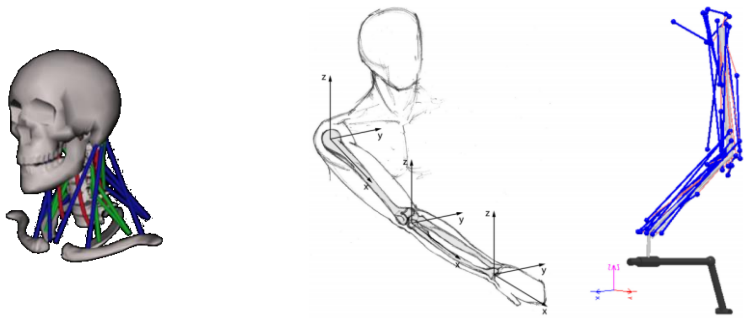

(a) Head-neck, from (Lee & Terzopoulos, 2006)

(b) Upper limb and helicopter collective lever from (Masarati & Quaranta, 2014)

Figure 3-5. Virtual human neuromusculoskeletal models

Early works in virtual human modeling and simulation can be found in (Maurel, 1999), in which even the modeling of soft tissues like skin is proposed. A skeletal model using a multibody approach using multibond graphs is proposed in (Martinez, Vera, & Félez, 1997). A formalization of the problem of the computation of human movement when excitation and the activation dynamics of muscles are taken into account is proposed in (Pandy, 2001) and (Pandy & Barr, 2003). A detailed upper limb musculoskeletal model is proposed in (Garner & Pandy, 2001), the positioning of muscle attachment points is particularly clear. In (Lee & Terzopoulos, 2006), a human head-neck biomechanical model is proposed. On top of the model, a multiple level neuromuscular control model is proposed; machine learning techniques are employed to train the neural networks of the controller to generate movements of the human head and face, see Figure 3-5. The impact and need to model control to obtain realistic arm impedance is discussed in (Stroeve, 1999) for which "*arm impedance is the resultant of passive dynamics of the arm, intrinsic impedance of activated muscles and reflexive contributions*". Usually, in these models known as "neuromusculoskeletal" represent to a certain extent the behavior of the three subsystems, skeleton, muscles and their control thanks to the central nervous system. However, these models of the human body are limited, since they do not take into account for example, muscle volume, or make the hypothesis that muscle forces are exerted along straight lines. These two hypothesis are not obvious to justify see Figure 3-6; more precise geometric reconstructions of muscles are proposed in (Ng-Thow-Hing, 2001) are muscle forces are exerted on more complex paths. These kind of physical details come at a higher computational cost.

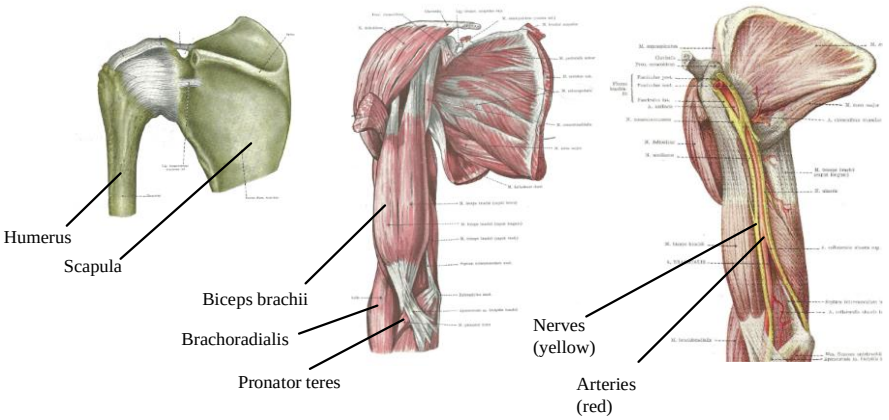

(a) Skeleton (b) Muscles (c) Nerves

Figure 3-6. Partial physiology drawings of the shoulder from (Kiss & Szentágothai, 1966)

In (Pennestri, Stefanelli, Valentini, & Vita, 2007) the mathematical model of a virtual musculoskeletal model that takes into account muscular activation dynamics of the upper limb is detailed in a reproducible way. These two models have been applied in (Masarati & Quaranta, 2014) to model the right arm of a helicopter pilot in order to compute a helicopter pilot BDFT in its vertical axis.

To synthetize, identification model approaches lead to black box models, which are usually linear and easy to be integrated by third parties in vehicle model analysis. However, they have a limited validity to the experiment in which they were identified. While approaches based on physical principles allow testing many more virtual situations. These more complex models could also have wider applications by contributing to the development of model-based estimation of muscle forces for clinical applications because they can provide "*insight into neural control and tissue loading and can thus contribute to improved diagnosis and management of both neurological and orthopedic conditions*" (Erdemir, McLean, Herzog, & van den Bogert, 2007).

Ideally, the prediction of biodynamic feedthrough would be a major contribution to improve rotorcraft designs. More precisely the prediction of envelops of BDFT that would represent the population of pilot involuntary behaviors in any flight configuration would be of interest. It could help, as early as possible in the design, to optimize the choice of design parameters and improve the design of the flight control system for a better robustness to PAOs.

3.2. Proposal

However, there has not yet been a consensus on how to model a human arm to compute biodynamic feedthrough as measured in experiments. The model proposed in this chapter is a combination of the models proposed in (Lee & Terzopoulos, 2006), (Pennestri, Stefanelli, Valentini, & Vita, 2007) and (Masarati & Quaranta, 2014). Its

originality is twofold, firstly the model is developed using bond graphs and secondly it is applied to the prediction of BDFT on the lateral axis of a conventional helicopter. While computing the left arm of a helicopter pilot movement that controls the collective lever, requires only representing a planar movement of the arm. In the present case of the right arm of the pilot, where he controls the cyclic lever, the arm movement is not planar anymore but spatial and the muscular repartition more asymmetrical; the resulting motion is therefore more complex. In the next sections the computation prediction of biodynamic feedthrough is described and then compared to literature experiments.

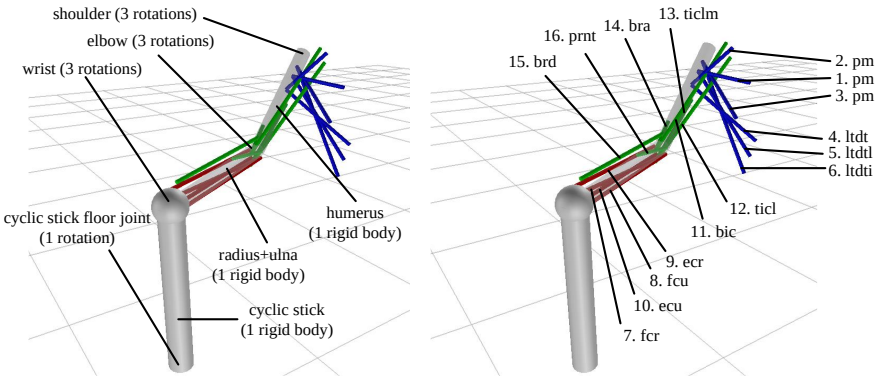

(a) Multibody system (b) Muscular system

Figure 3-7. Pilot's left upper limb neuromusculoskeletal system model proposal

Table 4. Muscle number and name of the proposed model

Muscle #	Abbrev	Name
between humerus and shoulder		
1	pm	pectoralis major (stern)
2	pm	pectoralis major (clav)
3	pm	pectoralis major (ribs)
4	ltdt	latissimus dorsi (thoracic)
5	ltdtl	latissimus dorsi (lumbar)
6	ltdti	latissimus dorsi (iliac)
between humerus and hand		
7	fcr	flexor carpi radialis
8	fcu	flexor carpi ulnaris
9	ecr	extensor carpi radialis
10	ecu	extensor carpi ulnaris

between radius and shoulder		
11	bic	biceps brachii caput l/b
between ulna and shoulder		
12	ticl	triceps brachii caput longus
between humerus and ulna		
13	ticlm	triceps brachii caput l/m
14	bra	brachialis
between humerus and radius		
15	brd	brachoradialis
16	prnt	pronator teres

3.3. Upper limb skeleton subsystem and closed kinematic loops

In the upper limb model developed in this work the forearm is considered to be directly attached to the cyclic stick, subtracting the presence of the hand. The arm is attached through the shoulder directly to the airframe, neglecting the motion of any supplementary limb. All the articulations are considered to be spherical joints and represent wrist, elbow and shoulder, see Figure 3-7. Each one of these joints degree of freedom contains stiffness and damping characteristics that are obtained from literature experimental identifications (Mattaboni, Fumagalli, Quaranta, & al., 2009). All the parameters and axes definitions of both *arm and cyclic lever* are presented on Appendix 4.The human forearm skeleton contains radius and ulna bones but it has been simplified to a single rigid body representing the characteristics of both bones. The humerus is also considered as a rigid body leading to a skeletal model of 2 rigid bodies and 9 degrees of freedom. The multibody model is developed using the approach presented in the previous chapter. When this skeleton subsystem is not attached to the cyclic stick it can be seen as a chain of bodies see Figure 3-8. However, once it is attached to the cyclic stick, both cyclic stick and arm are attached to the rotorcraft airframe leading to a multibody system that contains a closed kinematic chain (CKC) or loop on Figure 3-8. The computation of numerical solutions of multibody systems with a (CKC) is challenging because the topological loop (Figure 3-8) leads to equations of motion in the form of DAEs of a higher index[14] than 2, usually 3, see (Dabney, 2002) .

[14] Index: number of times the constraint equation has to be differentiated to obtain a system of ODEs (Van Dijk & Breedveld, Simulation of system models containing zero-order causal paths—I. Classification of zero-order causal paths, 1991)

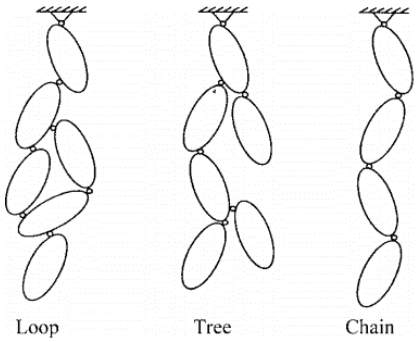

Figure 3-8. Topology of multibody systems from (Eberhard & Schiehlen, 2006)

While this higher index DAEs can be theoretically solved numerically, most numerical methods implemented in commercial software might not be able to solve them. Many methods exist to circumvent the problem based on the manipulation of equations (Boudon, 2014). Another approach, known as the singular perturbation method (Zeid & Overholt, Singularly Perturbed Formulation: Explicit Modeling Of Multibody Systems, 1995), (Boudon, 2014) consists in reworking the hypothesis of the system model at the physical level. This approach is chosen in this work since it can be controlled at the bond graph level in a systematic way. The approach consists in breaking the kinematic loop constraint by replacing at least one rigid constraint of the loop with a stiff compliance and a damping term; the index of the DAE is reduced but a 'stiff' ordinary differential equation is added to the system that can be efficiently solved numerically in 20-sim® using the integrated Backward Differentiation Formula (BDF) method. In our application, this approach is implemented by breaking the rigid translation velocity constraint of the revolute joint between the cyclic stick and the airframe at the bond graph level see, Figure 3-9.

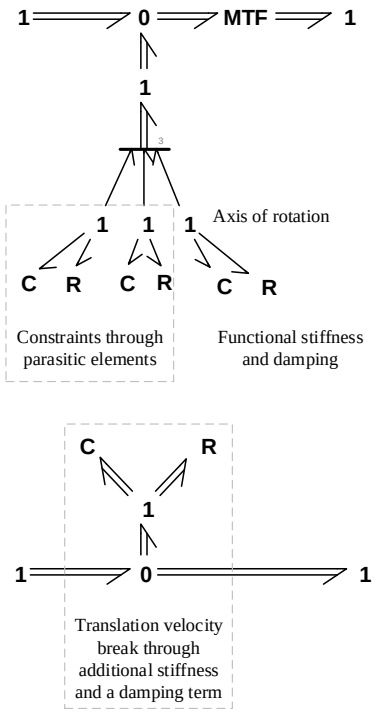

Figure 3-9. 'Breaking' the translation velocity constraint of a revolute joint

This method has the disadvantage, as already stated in the previous chapter, of introducing new state variables and therefore new modes that will perturb the analysis of the system. In addition, there is no systematic method to choose the value of stiffness and damping of these elements. The advantage of this method is that it can be implemented at a physical level in a systematic way by the modeler whether analytically or at the bond graph level.

3.4. Hill-type muscle forces subsystem

The human upper limb contains more than 60 muscles but in this first approach only 16 will be represented, see Figure 3-7 and Table 4. Prior to further complexification, experimental confrontation of the actual model is needed to verify muscles forces and kinematic predictions. Once the skeletal model is in place, muscles can be superposed to the multibody system. In this section, a bond graph representation of a Hill-type muscle (Zajac, 1988) as developed analytically in (Pennestri, Stefanelli, Valentini, & Vita, 2007) is proposed. In (Wojcik, 2003), a Hill-type muscle is represented using bond graphs by a source of effort; however neither the explicit expression of the force and the computation of activation dynamics are presented, making it impossible to be used. The particularity of the model proposed in this section is that it allows taking into account spatial motion of the skeleton which is essential in our application. As

described in (Pennestri, Stefanelli, Valentini, & Vita, 2007), Hill-type muscle force models can be decomposed into an active and a passive component,

$$F_{muscle} = F_a + F_p \tag{37}$$

The active component generates a force that depends on the muscle length, its contraction velocity and its muscular activation function *a(t)* "*which assumes a value between 0 and 1 (0 for not-activated and 1 for fully activated muscle)*" (Pennestri, Stefanelli, Valentini, & Vita, 2007). The passive component depends on the muscle length only.
Nondimensional muscle length *x* and muscle contraction velocity *v* are defined as,

$$x = \frac{l(t)}{l_0} \text{ and } v = \frac{\dot{l}(t)}{v_{\max}} \tag{38}$$

Where v_{max} is the maximum contraction velocity chosen as muscle independent and to be equal to 2.5 m/s (Pennestri, Stefanelli, Valentini, & Vita, 2007). By introducing, the maximal muscle force scalar f_0, the functions f_1 and f_3 that depend on muscle length *l(t)*, and f_2 that takes into account muscle forces that vary with muscle length, muscle stretching velocity and their activation the muscle force is expressed as,

$$F_{muscle} = f_0\left(f_1(x) f_2(v) a + f_3(x)\right) \tag{39}$$

Where each function is,

$$\begin{aligned} f_1(x) &= e^{-40(x-0.95)^4+(x-0.95)^2} \\ f_2(v) &= 1.6\left(1-e^{-1.1/(1-v)^4+0.1/(1-v)^2}\right) \\ f_3(x) &= 1.3\arctan\left(0.1\left(x-0.22\right)^{10}\right) \end{aligned} \tag{40}$$

On Figure 3-10, the nondimensional muscle force is plotted for a fully activated and not-activated muscle; in this last case, the purely elastic characteristic of the muscle can be observed.

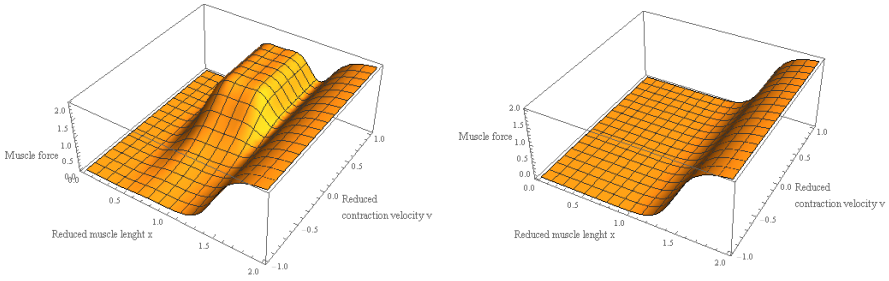

(a) Fully activated muscle, $a=1$ (b) Not-activated muscle, $a=0$

Figure 3-10. Muscle force length and velocity relationships
$f_1(x)f_2(v)a+f_3(x)$

In application to the representation of the first muscle of the proposed model in this work, which is *pectoralis major*, see Figure 3-7, the bond graph representation of a muscle derivation is developed below. First let us define the muscle force line of action,

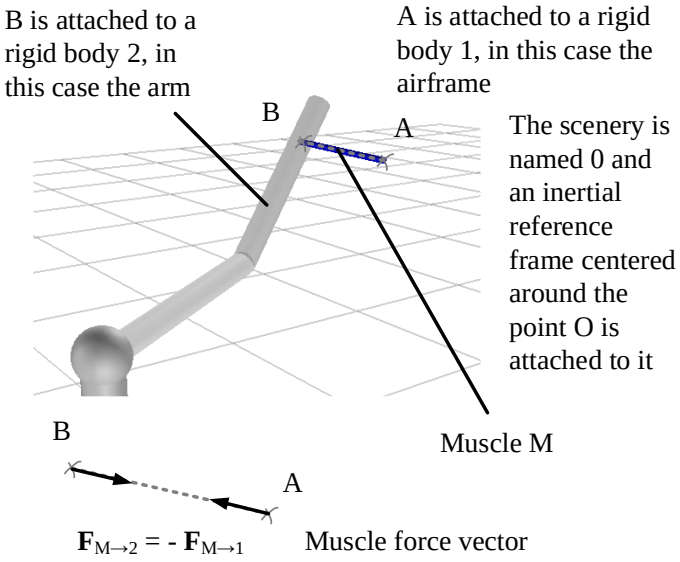

Figure 3-11. Muscle force vector definition between two rigid bodies in spatial motion

Since the muscle force vector norm depends on muscle length $l(t)$ and stretch velocity (total time derivative of $l(t)$), these two quantities need to be expressed in a bond graph exploitable way,

$$l(t) = \|\mathbf{AB}(t)\| \tag{41}$$

$$\begin{aligned}\mathbf{AB} &= \mathbf{AO} + \mathbf{OB} \\ &= -\int\left(\frac{d}{dt}^{0}\mathbf{OA}\right)dt + \int\left(\frac{d}{dt}^{0}\mathbf{OB}\right)dt\end{aligned} \tag{42}$$

The above total time derivatives in the inertial reference frame are introduced to let appear the velocities of the points A and B with respect to the inertial reference frame. By definition,

$$\frac{d}{dt}^{0}\mathbf{OA} = \mathbf{V}_{A,1/0} \tag{43}$$

$$\frac{d}{dt}^{0}\mathbf{OB} = \mathbf{V}_{B,2/0} \tag{44}$$

These velocities are bond graph flows that naturally appear in the multibond graph representation of a rigid body, see Figure 2-5 and the explanations associated in that section. The muscle length can therefore be expressed,

$$l(t) = \left\|\int\left(\mathbf{V}_{B,2/0} - \mathbf{V}_{A,1/0}\right)dt\right\| \tag{45}$$

By previous definitions, Figure 3-11 and knowing that f_0, f_1, f_2 and f_3 are positive definite functions,

$$\mathbf{F}^{0}_{M\to 2} = -f_0\left(f_1 f_2 a + f_3\right)\frac{\mathbf{AB}^{0}(t)}{\left\|\mathbf{AB}^{0}(t)\right\|} \tag{46}$$

The equations at the zero junctions of the multibond graph structure proposed on Figure 3-12 which is quite similar to the classic Hill-type schematic muscle structure leads to,

$$\mathbf{F}^{0}_{M\to 2} = \mathbf{F}^{0}_{PE} + \mathbf{F}^{0}_{CE} \tag{47}$$

With the expressions of the contractile and parallel element forces as functions of their incoming bond flows,

$$\begin{aligned}\mathbf{F}^{0}_{CE} &= -f_0 f_1 f_2 a\frac{\mathbf{AB}^{0}(t)}{\left\|\mathbf{AB}^{0}(t)\right\|} \\ &= -f_0 f_1 f_2 a\frac{\int\left(\mathbf{V}^{0}_{B,2/0} - \mathbf{V}^{0}_{A,1/0}\right)dt}{\left\|\int\left(\mathbf{V}^{0}_{B,2/0} - \mathbf{V}^{0}_{A,1/0}\right)dt\right\|}\end{aligned} \tag{48}$$

$$\begin{aligned}\mathbf{F}^{0}_{PE} &= -f_0 f_3\frac{\mathbf{AB}^{0}(t)}{\left\|\mathbf{AB}^{0}(t)\right\|} \\ &= -f_0 f_3\frac{\int\left(\mathbf{V}^{0}_{B,2/0} - \mathbf{V}^{0}_{A,1/0}\right)dt}{\left\|\int\left(\mathbf{V}^{0}_{B,2/0} - \mathbf{V}^{0}_{A,1/0}\right)dt\right\|}\end{aligned} \tag{49}$$

In order to be able to say that the parallel element of the muscle is a C element, and that it is energy conservative, it has to verify the *Maxwell reciprocity condition* (Borutzky, 2009). By using standard, bond graph definitions, a C element storage element is defined by the function[15] $\boldsymbol{\Phi}_C$ relating the effort vector $\boldsymbol{e}$ to the generalized displacement vector $\boldsymbol{q}$,

$$\mathbf{e}(t) = \boldsymbol{\Phi}_C^{-1}(\mathbf{q}(t)) \tag{50}$$

The *Maxwell's reciprocity condition* implies that for $i \neq j$,

$$\frac{\partial e_i}{\partial q_j} = \frac{\partial e_j}{\partial q_i} \tag{51}$$

In our case the generalized displacement vector can be expressed by,

$$\mathbf{q}(t) = \int flow.dt = \int \left(\mathbf{V}_{B,2/0}^0 - \mathbf{V}_{A,1/0}^0 \right) dt = \mathbf{AB}^0(t) \tag{52}$$

Therefore the inverse of the function Φ_C can be expressed as,

$$\boldsymbol{\Phi}_C^{-1}(\mathbf{q}) = \frac{f_0 \cdot f_3\left(\frac{\sqrt{\mathbf{q}^T.\mathbf{q}}}{l_0} \right)}{\sqrt{\mathbf{q}^T.\mathbf{q}}} \mathbf{q} \tag{53}$$

Finally one can verify with the help of a formal computation software such as Mathematica® that for $i \neq j$, the equality below is verified and that the parallel element behavior of the muscle can be modeled as a bond graph C element,

$$\frac{\partial}{\partial q_j}\left(\frac{f_0 \cdot f_3\left(\frac{\sqrt{\mathbf{q}^T.\mathbf{q}}}{l_0} \right)}{\sqrt{\mathbf{q}^T.\mathbf{q}}} q_i \right) = \frac{\partial}{\partial q_i}\left(\frac{f_0 \cdot f_3\left(\frac{\sqrt{\mathbf{q}^T.\mathbf{q}}}{l_0} \right)}{\sqrt{\mathbf{q}^T.\mathbf{q}}} q_j \right) \tag{54}$$

[15] Mechanically speaking, modeling a spring with a linear constant stiffness characteristic k would simply lead to $\Phi_C^{-1}(q) = k$, such that the spring force equal to $\Phi_C^{-1}(q).q$

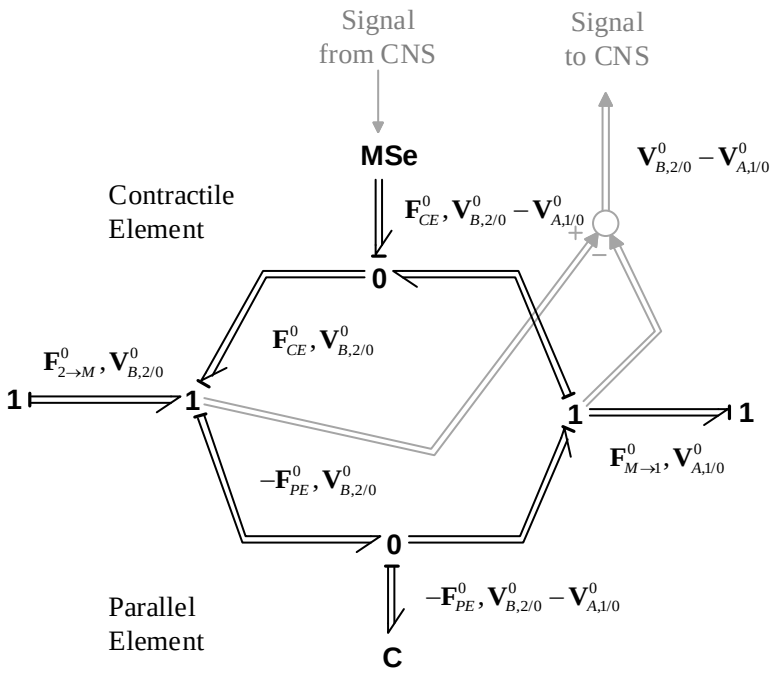

Figure 3-12. Hill-type muscle structure proposal using multibond graphs

In terms of energy, the total work that muscle forces input in the system can be computed by summing the energy at the root of the modulated source of effort (MSe) and the capacitance (C). Each muscle force work expression is given by,

$$W_{muscle} = \int \left(\mathbf{F}^0_{CE} - \mathbf{F}^0_{PE}\right).\left(\mathbf{V}^0_{B,2/0} - \mathbf{V}^0_{A,1/0}\right) dt \tag{55}$$

Since human body motion can only be achieved by the power given by muscle forces, this quantity represents the energetic cost for the organism to generate the motion. However this quantity represents only a part of the energy cost for our body to move, because in the process, muscles also heat. Summing all the energetic costs for the body to generate motion leads to what is called metabolic cost. The dissipation of energy due to heating is not negligible (Schiehlen, 2006). However, our interest in metabolic cost will be to minimize it rather than trying to obtain realistic values of it. As a result, it is reasonable to think that minimizing metabolic cost is equivalent to minimizing W_{muscle}.

3.5. Central nervous system (CNS) control subsystem

In addition to the musculoskeletal system, the reflex control of the muscles by the central nervous system is taken into account. The reflex control model proposed in (Lee & Terzopoulos, 2006), (Masarati & Quaranta, 2014) reproduce the variation of muscular activation Δa that depends on the muscle length and the muscle contraction velocity. This section model is the one that has been developed in (Lee & Terzopoulos, 2006) as part of the neural control system of a neck face model 'to synthesize a variety of autonomous movements for the behavioral animation of the human head and face', see Figure 3-13.

Figure 3-13. Neuromuscular control of the neck from (Lee & Terzopoulos, 2006)

The variation of muscular activation Δa is due to the feedback control that is represented in gray on Figure 3-12 such that,

$$a = a_0 + \Delta a \tag{56}$$

Where a_0 is an initial muscle activation coefficient and Δa is a quasi-steady variation around it such that, by introducing the muscle reflexive feedback gain on muscle length k_p; and the reflexive feedback gain on muscle contraction velocity k_v,

$$\Delta a = k_p.x + k_v.v \tag{57}$$

In addition a function is defined such that if $a_0+k_px+k_vv<0$ then $a=0$ and if $a_0+k_px+k_vv>1$ then $a=1$. In this way, a can only take a value between 0 and 1, respecting the definition of activation given previously.

3.6. Minimizing metabolic cost to compute muscular activation coefficients

The human musculoskeletal system possesses more muscles than degrees of freedom; as a result it is over actuated. And since each muscle force depends on its activation, the over actuation leads to a mathematical indeterminacy (Pandy, 2001), (Erdemir, McLean, Herzog, & van den Bogert, 2007): there are more unknowns than equations and the problem has an infinity number of solutions. However when a human tries to grab an object with his arms, it seems he always find one similar solution to go from your initial arm position to the 'object grabbed' position. After experimental work,

scientists have hypothesized that the human body tries to minimize its energy consumption or metabolic cost during walking (Zarrugh, Todd, & Ralston, 1974), it is also proposed to be a principle governing neuronal biophysics in (Hasenstaub, Otte, Callaway, & Sejnowski, 2010). The addition of this principle of minimization of metabolic cost allows solving the indeterminacy and computing muscle activation coefficients (Erdemir, McLean, Herzog, & van den Bogert, 2007). This is not the only way of solving the indeterminacy problem; another very popular minimization is the one of muscle stress (Erdemir, McLean, Herzog, & van den Bogert, 2007). The same work proposes a review of the different techniques that can be employed to compute muscle forces or muscle excitations see Figure 3-14.

In A, the objective is to obtain the equivalent muscle forces that need to appear in the musculoskeletal model to match with joint torques that are the output of experimental kinematic measures through an inverse dynamics model; "*muscle forces are iteratively updated by an optimization scheme until the objective function J (e.g. total muscle stress) is minimized and equality constraints between experimental joint torques and muscular moments are satisfied*" (Erdemir, McLean, Herzog, & van den Bogert, 2007). In B, the objective is to obtain muscular excitations. In the previous section, the notion of muscle activation has been introduced, however "*muscles cannot be activated or relaxed instantaneously*" (Pandy, 2001). A time delay appears between muscle excitation and muscle activation due to the chemical process between the two events. As a result, this dynamic might be represented (Pandy, 2001).

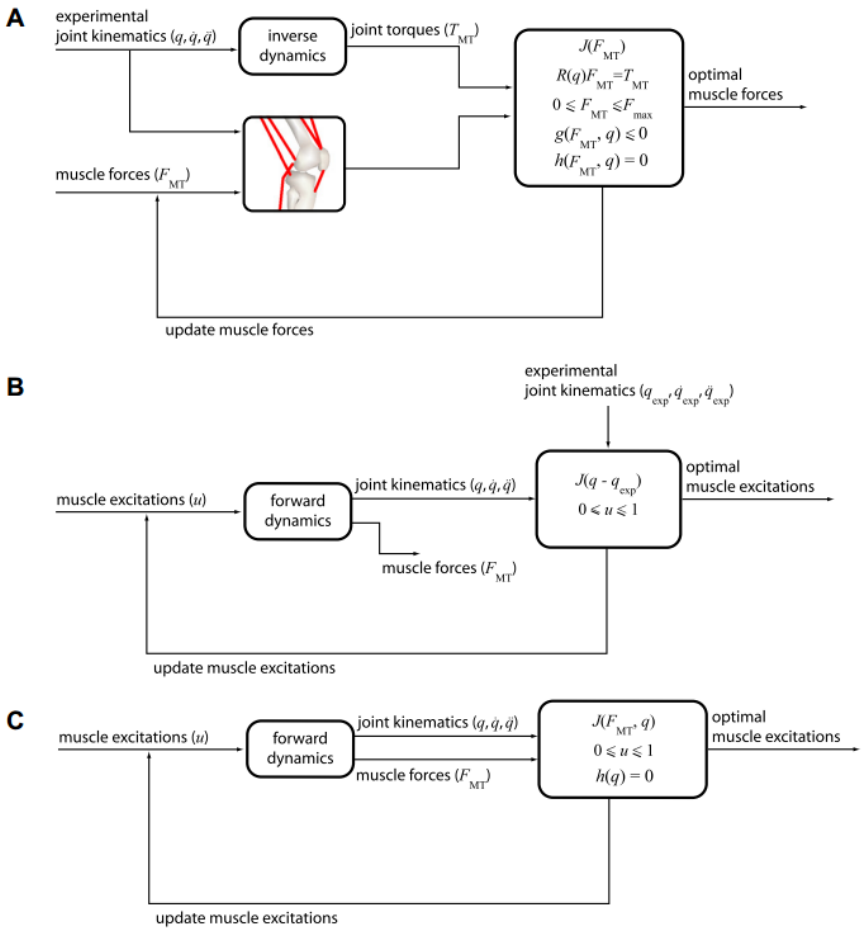

Figure 3-14. Model-based estimation of forces or excitations from (Erdemir, McLean, Herzog, & van den Bogert, 2007)

In this work, this time delay has not been taken into account; the C approach of Figure 3-14 is applied, see Figure 3-15.

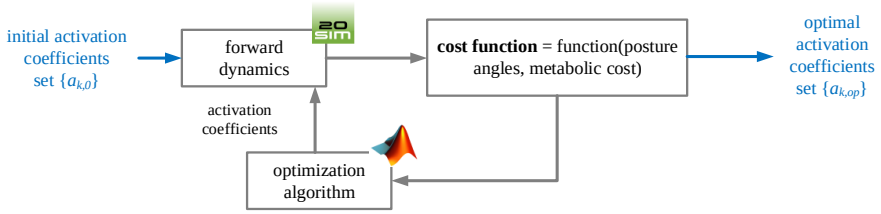

Figure 3-15. Applying a forward dynamics approach to determine muscular activation coefficients

It consists in determining optimal activation coefficients for a given posture and reflex control setting by minimizing a cost function that depends both on the upper limb bone angles and metabolic as proposed in (Brouwn, 2000). In that work the following cost function *J* is proposed,

$$J = \int_0^t \left\{ q.\left[x(t) - x_d(\mathrm{t}) \right]^2 + p.u^2(t) \right\} dt \tag{58}$$

Where x is the vector of positions, x_d is the vector of desired equilibrium or posture and u the control signal. The metabolic energy consumption is modeled by u^2. In this case, p and q weighing factors parameter the strategy adaption of the central nervous system to achieve an objective (Brouwn, 2000). In our work, the weighing factors are set to 1, not to privilege any strategy, and the metabolic energy consumption is replaced by the muscles forces work that can be naturally computed from the bond graph, see equation (55) and the paragraph associated. The cost function J becomes therefore,

$$J = \int_0^t \left\{ \left[x(t) - x_d \right]^2 + \left(\sum_i W_{muscle\ i}(t) \right)^2 \right\} dt \tag{59}$$

In this work, see Figure 3-15, the optimization function that is used is *fminsearch* from Matlab®, to find the minimum of unconstrained multivariable nonlinear functions using a derivative-free method. Since the muscular activation coefficients need to be constrained between 0 and 1, the absolute value of the sinus of the results proposed by Matlab® are the muscular activation coefficients that are sent for simulation to the bond graph physical model implemented in 20-sim®. More efficient and adapted optimization functions could be used, for example by providing also the derivative of the cost function, but out of the scope of this work.

3.7. Biodynamical model validity

In the previous section an upper limb neuromusculoskeletal model was developed with the objective of predicting numerically the biodynamic feedthrough (BDFT) of a helicopter pilot on its lateral axis.

As a remainder of the beginning of the chapter, in (Venrooij, et al., 2011) BDFT measures on helicopter flight simulators lateral axis are presented. In that experiment, BDFT of different subjects were measured when asked to perform different control tasks. The objective of asking one subject to perform different tasks is to force him to adapt his body and therefore his neuromuscular system to the task. The results are presented on Figure 3-4 for the lateral, longitudinal and vertical helicopter axis translations and show that BDFT is also task dependent. The subjects were asked to perform three tasks. A position task (PT) with the instruction to minimize the position of the stick, a force task (FT) with the instruction to minimize the force applied to the stick and finally a relax task (RT) with the instruction to relax the arm. Trying to characterize the arm response can be interpreted as trying to characterize its impedance. In (Stroeve, 1999) for which "*arm impedance is the resultant of passive dynamics of the arm, intrinsic impedance of activated muscles and reflexive contributions*".

In order to reproduce a given task, which is conjectured to correspond to a neuromuscular system set, the variation of two parameters is discussed in the next paragraphs, which are the reflexive feedback gain on muscle length *kp* and a multiplication coefficient on wrist and elbow passive stiffness and damping characteristics denoted α. Once these two parameters are chosen, the forward dynamics approach described in previous sections is launched to obtain optimal muscular activation coefficients. The results are presented on Figure 3-16 where *kp* and α are gradually increased. It does not to be a consensus in literature on which parameters should be varied to parameter a given neuromuscular set.

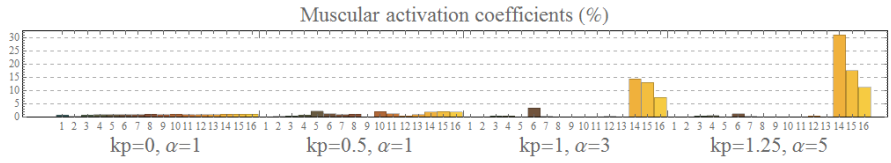

Figure 3-16. Arm muscular activation coefficients computation for each one of the 16 muscles

Interestingly, the optimization converges to the need for the upper limb of the pilot model to activate more importantly muscles 14, 15 and 16 which correspond to *brachialis* (30%), *brachoradialis* (20%) and *pronator teres* (10%). These three muscles connect the humerus to the ulna and radius, see Figure 3-6 and Figure 3-7. In other words for given variations of position and velocity between the forearm and the arm of the pilot, these muscles produce higher forces when increasing reflexive feedback *kp* and passive characteristics of wrist and elbow joints coefficient α.

The obtained muscle activation coefficients for different setups of the pilot neuromuscular system are conjectured to represent pilot task variability. For each task

or neuromuscular system setup, the next step of the numerical experiment consists in computing the lateral BDFT; which is the cyclic stick lever angle divided by the imposed sinusoidal airframe accelerations on its lateral axis that vary from 0.8 to 8 Hz. On Figure 3-17, the results of two simulations are presented for two sets of parameters for α and *kp*. On Figure 3-18, the numerical experiment described above is performed also without the pilot; the result in gray points shows simply the behavior of a second order mass-spring system that corresponds to the oscillations of the cyclic stick with no pilot action. The inclusion of the pilot in the system modifies the shape of this behavior as it can be seen on Figure 3-18.

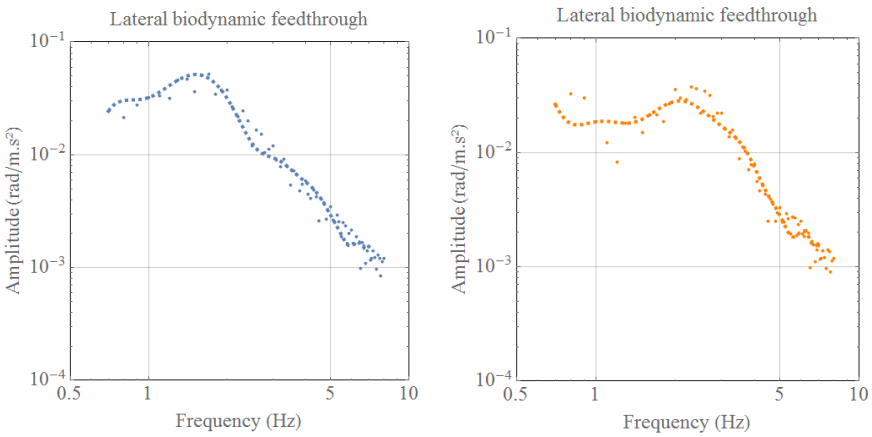

(a) kp=0, α=1, least square approximation

(b) kp=1.25, α=5, least square approximation

Figure 3-17. BDFT Numerical simulation results

The increase of α from 1 to 5 shifts the resonant frequency and decreases the amplitude of BDFT at this same frequency. This is understandable since, increasing α is equivalent to an increase of wrist and shoulder stiffness, which at constant mass and inertia leads to a higher resonant frequency. The increase of α also leads to an increase of wrist and shoulder local damping moments for which the decrease of amplitude of BDFT can be explained. The impact of modifying *kp*, which parameters the reflexive muscle length feedback coefficient of the activation has especially an impact at lower frequencies, below 1 Hz where harmonics appear with high gains see Figure 3-20. The increase in reflexive feedback also impacts the shape of BDFT around the resonant frequency see (b) Figure 3-17.

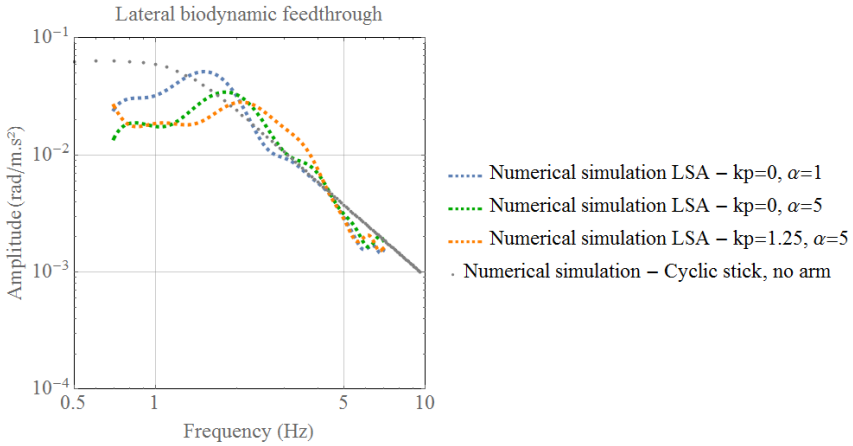

Figure 3-18. BDFT Numerical simulations evolution with and without pilot

On Figure 3-19 (a), the proposed set of parameters leads to a BDFT resonant frequency that is higher from what has been found in the experiment. This is not surprising when taking into account that the pilot model parameters of mass, inertia, stiffness and damping characteristics come from subject identification experiments that are not related with this BDFT experimental measures. On Figure 3-19 (b), the increase of *kp* has allowed to maintain a high amount of gain at lower frequencies than resonant frequency which seems to correspond to what has been observed during the experiment.

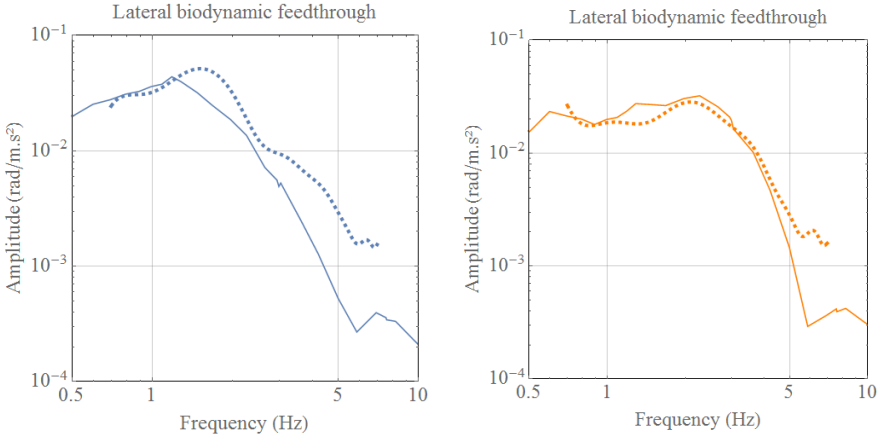

(a) experimental force task (FT) (–) simulation *kp*=0, *α*=1 (--)

(b) experimental position task (PT) (–) simulation *kp*=1.25, *α*=5 (--)

Figure 3-19. BDFT experimental results from (Venrooij, et al., 2011) vs. numerical simulation results

Finally the comparison presented on Figure 3-19 is encouraging. However, in general, additional experiments are needed to identify consistent pilot model parameters of mass, inertia, stiffness and damping characteristics of the upper limb with the subjects that actually were in the cockpit of the flight simulator experiment. In terms of BDFT identification, Figure 3-17 (a) and (b) are sections of Figure 3-20. For the (b), the model is clearly nonlinear see the peaks on (b) Figure 3-20.

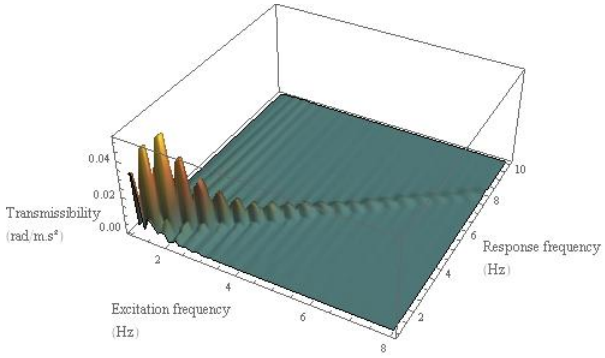

(a) kp=0, α=1

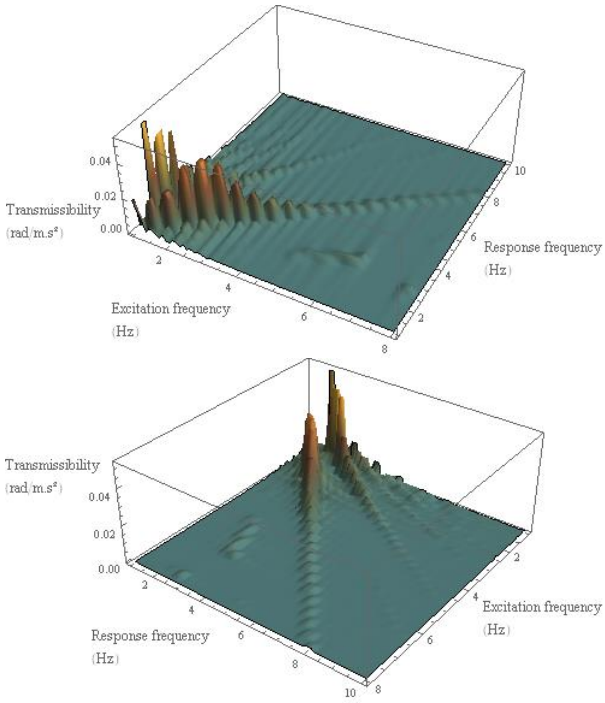

(b) kp=1.25, α=5 (two different views)

Figure 3-20. Numerical simulation, BDFT Spectrograms

The hypothesis of taking the BDFT as a section at those low frequencies seems to be very reductive. This could be addressed, by comparing complete BDFT spectrograms and not just sections from both simulation and experiment. In addition, the modelling of the interfaces at the level of the wrist and the shoulder needs probably to be more detailed since the muscular activation of the muscles around these zones seem extremely low. In particular the deltoid muscle has not been modeled, see Figure 3-21. Once this is done, it would be interesting to see if α coefficient still plays a significant role in the shift of BDFT resonant frequency.

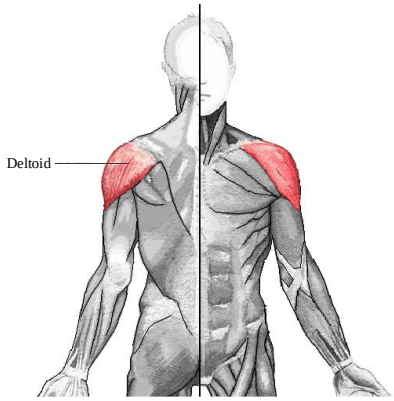

Figure 3-21. Deltoid muscle position

3.8. Conclusion

In this chapter a pilot model has been developed. It consists in a neuromusculoskeletal model of pilot's left upper limb. The individual subsystems that compose this model have been taken from literature. However, multibond graph representations are proposed for the first time to model individual muscles that produce force between bones that have spatial motion. This model is applied on the first time for the prediction of BDFT on the lateral axis of a helicopter.

It is known that the computation of the motion of human movement or posture leads to a mathematical indeterminacy because the human body possesses less degrees of freedoms than muscles that act as actuators that can only contract. It has been pointed out as proposed in literature, that the addition of an energetic principle can solve the indeterminacy problem. It consists in postulating that the human body minimizes metabolic cost during motion. From a computational point of view an optimization algorithm is used to minimize muscle forces work which can be computed naturally by the energetic representation given by bond graphs. This allows to obtain the muscular activation coefficients around several neuromuscular settings.

The system represented in this chapter has also the particularity of being closed, kinematically speaking. The simulation of such systems is challenging; the singular perturbation method can be locally applied at the graphical level in a systematic manner to reduce the index of the DAEs prior to a resolution with a commercial

solver. This method has however the disadvantage of introducing new state variables and therefore new modes that will perturb the analysis of the system.

Finally numerical simulations are performed to compute pilot's biodynamic feedthrough (BDFT). The results are quite encouraging and allow to find similar qualitatively similar gain values to literature experiments. The task dependency of helicopter pilots BDFT can be predicted to a certain extent. As a manner of fact, an iterative procedure has allowed to find a set of parameters that have a physical meaning to reproduce what has been seen in experiments.

In the short term, the model prediction in terms of kinematics should be compared to other literature models and supplementary experiments. In the long term, the next step would be to find an explicit mathematical relation between task and neuromuscular system parameters. This would allow obtaining a useful quantity for rotorcraft designers which would be BDFT maximal envelops rather than precise BDFT pilot behaviors.

In synthesis, the reader should remember the BDFT of a given human being depends on the settings of his neuromuscular system; for example whether he/she is stressed or not.

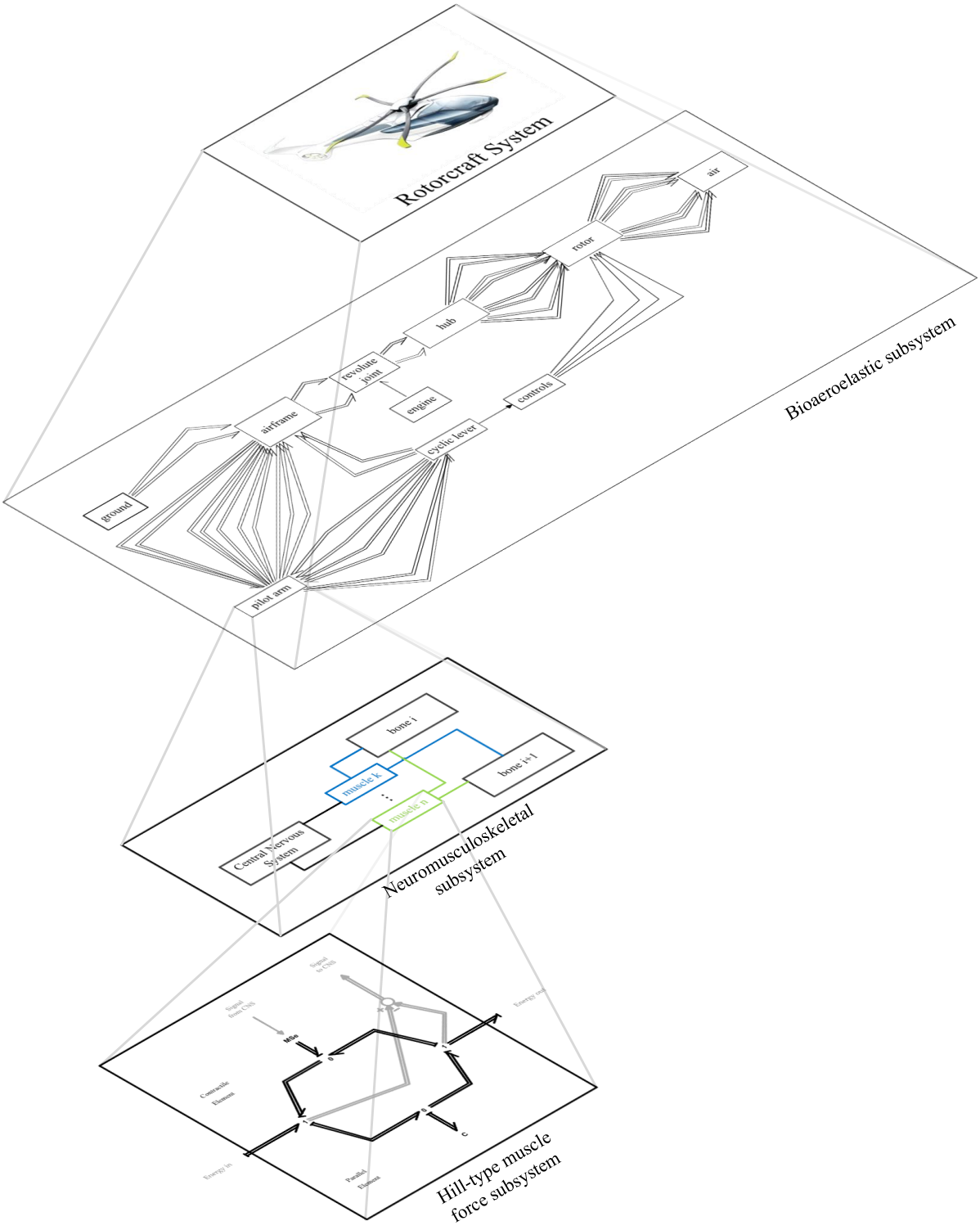

Figure 3-22. Chapter 3 main modeling blocks contribution to the global modeling approach